ISSN 1070-3632, Russian Journal of General Chemistry, 2019, Vol. 89, No. 11, pp. 2273–2284. © Pleiades Publishing, Ltd., 2019.
Russian Text © The Author(s), 2019, published in Zhurnal Obshchei Khimii, 2019, Vol. 89, No. 11, pp. 1766–1779.

Double Pseudo-Polymeric Gold(III)–Mercury(II) Complexes $[Au(S_2CNR_2)_2]_nX$ [$R_2 = (CH_2)_6$, $(CH_2)_4O$] Containing $([HgCl_3]^-)_n$, $[HgCl_4]^{2-}$, and $[Hg_2Cl_6]^{2-}$ Anions: Chemisorption Synthesis, Principles of Supramolecular Self-Assembly, and Thermal Behavior

O. V. Loseva[a], T. A. Rodina[a], and A. V. Ivanov[a,*]

[a] *Institute of Geology and Nature Management, Far Eastern Branch of the Russian Academy of Sciences, Blagoveschensk, 675000 Russia*
**e-mail: alexander.v.ivanov@chemist.com*

Received April 19, 2019; revised April 19, 2019; accepted for publication May 17, 2019

Abstract—Novel pseudo-polymeric complexes of gold(III)–mercury(II) with cyclic alkylene dithiocarbamate ligands: $([Au\{S_2CN(CH_2)_6\}_2][HgCl_3])_n$, $([Au\{S_2CN(CH_2)_6\}_2]_2[HgCl_4]\cdot H_2O)_n$, and $([Au\{S_2CN(CH_2)_4O\}_2]_2[Hg_2Cl_6])_n$ have been obtained and structurally characterized. The sophisticated supramolecular structure of the obtained compounds is realized due to secondary non-valent Au···S interactions and includes mononuclear and binuclear cations and anions as structural units as well as cationic and anionic polymer chains. The thermal behavior of the obtained complexes has been studied by means of simultaneous thermal analysis. The products of thermal transformations of the complexes are reduced elemental gold and $HgCl_2$.

Keywords: mercury(II) dithiocarbamates, chemisorption activity, gold(III)–mercury(II) dithiocarbamato-chlorido complexes, supramolecular self-assembly

DOI: 10.1134/S1070363219110185

Dithiocarbamates and their derivatives have been widely used in industry for flotation enrichment of sulfide ores (as collecting reagents) [1] and in the production of rubber (as curing additives) [2]. Metal dithiocarbamates are convenient precursors for the preparation of semiconducting nanocrystalline powders and films of metal sulfides [3–8], as well as heterometallic sulfides [9]. Gold(III) complexes with dithiocarbamate ligands have exhibited antitumor activity [10–12], whereas gold(I) dithiocarbamates have revealed luminescent properties [13, 14].

We have earlier prepared and characterized the structure of a series of dithiocarbamate mercury(II) complexes: $[Hg_2(S_2CNR_2)_4]$ {$R_2 = (CH_2)_6$ [15], $(CH_2)_5$ [16]; R = *iso*-C_3H_7 [17]} and $[Hg\{S_2CN(CH_2)_4O\}_2]_n$ [18].[1] Moreover, the study of the interaction between mercury(II) dithiocarbamates with gold(III) has revealed the efficient binding of the latter from the solutions into the solid phase with the formation of supramolecular heteronuclear Au(III)–Hg(II) complexes [16, 17, 21].

This study aimed to evaluate the chemisorption activity of mercury(II) complexes with cyclohexamethylene- and morpholinedithiocarbamate ligands with respect to $[AuCl_4]^-$/HCl (2 M), to isolate the Au(III)–Hg(II) complexes as individual forms of bound gold, and to investigate their structure and thermal behavior.

Double ionic-polymeric compounds $([Au\{S_2CN(CH_2)_6\}_2]\cdot[HgCl_3])_n$ (**1**), $([Au\{S_2CN(CH_2)_6\}_2]_2[HgCl_4]\cdot H_2O)_n$ (**2**), and $([Au\{S_2CN(CH_2)_4O\}_2]_2[Hg_2Cl_6])_n$ (**3**) were prepared via chemisorption of gold(III) from hydrochloric acid solutions by mercury(II) dithiocarbamate complexes. Freshly prepared mercury(II) cyclohexamethylene- and morpholinedithiocarbamates were curdled light-yellow precipitates, having a highly developed surface. As per scanning electron microscopy data, they consisted of

[1] The systematization of structurally characterized dithiocarbamate mercury(II) complexes has been previously described in detail [19, 20].

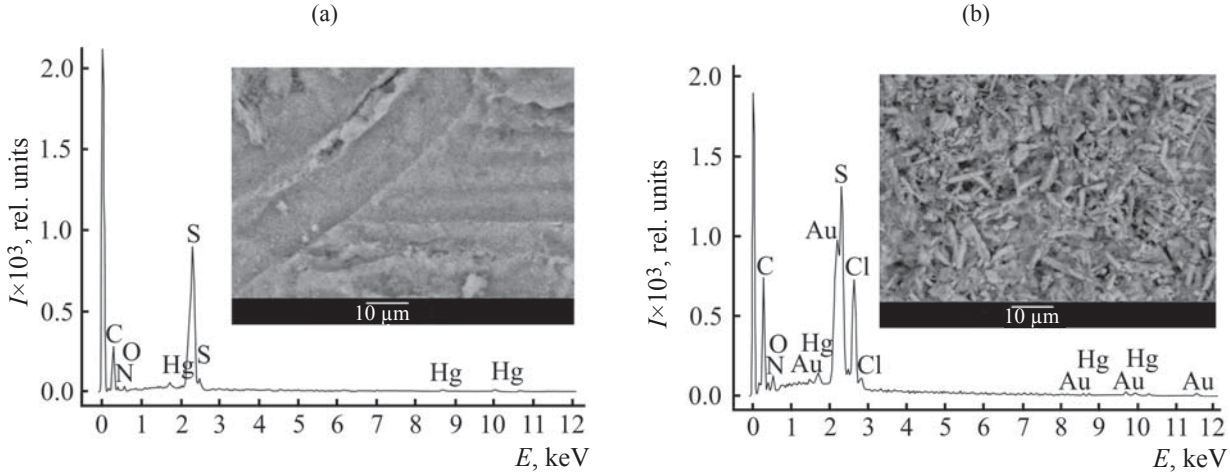

Fig. 1. Particles size and shape and energy-dispersive spectra of the $[Hg\{S_2CN(CH_2)_4O\}_2]$ (a) and $[Au\{S_2CN(CH_2)_4O\}_2]_2[Hg_2Cl_6]$ (b) complexes.

sphere-like particles with diameter of 0.5 μm; the energy-dispersive spectra reflecting the qualitative composition of the starting complexes contained the peaks of Hg, C, N, and S (see the data for $[Hg\{S_2CN(CH_2)_4O\}_2]_n$ in Fig. 1a). The interaction of mercury(II) dithiocarbamates with $H[AuCl_4]$ solutions was accompanied by the rapid change in the sorbents color to intense-yellow within several minutes, the surrounding solutions being simultaneously discolored. The shape of the precipitate particles was changed from spherical to elongated (6.8–8.3 μm, diameter 1.4–2.5 μm). The energy-dispersive spectra of the products evidenced the presence of Au and Cl (Fig. 1b). The change in the chemical composition of the complexes upon the chemisorption of gold from the solution directly confirmed the formation of the Au(III)–Hg(II) heteronuclear compounds in the studied systems.

Chemisorption interaction of mercury cyclohexamethylenedithiocarbamate with $H[AuCl_4]$ mainly led to the formation of compound **1** as platelet crystals, along with needle-like crystals of complex **2**. Hence, the binding of gold(III) from the solution could be expressed by the heterogeneous reactions (1) and (2).

$$[Hg_2\{S_2CN(CH_2)_6\}_4] + 2H[AuCl_4] = 2[Au\{S_2CN(CH_2)_6\}_2][HgCl_3]\ (\mathbf{1}) + 2HCl, \quad (1)$$

$$[Hg_2\{S_2CN(CH_2)_6\}_4] + 2H[AuCl_4] = [Au\{S_2CN(CH_2)_6\}_2]_2[HgCl_4]\ (\mathbf{2}) + HgCl_2 + 2HCl. \quad (2)$$

The binding of gold(III) with $[Hg\{S_2CN(CH_2)_4O\}_2]_n$ gave complex **3** [reaction (3)].

$$2[Hg\{S_2CN(CH_2)_4O\}_2] + 2H[AuCl_4] = [Au\{S_2CN(CH_2)_4O\}_2]_2[Hg_2Cl_6]\ (\mathbf{3}) + 2HCl. \quad (3)$$

Reactions (1) and (3) could be formally reduced to chemisorption binding of an $AuCl_3$ molecule with each mononuclear $[Hg(S_2CNR)_2]$ fragment of the complexes. In the case of reaction (2), binding of gold(III) was accompanied by partial ion exchange and release of 1/2 of mercury(II) in the solution.

IR spectra of the studied crystalline complexes contained strong single absorption bands at 1522 (**1**) and 1537 (**3**) cm^{-1} assigned to the N–C(S)S bonds stretching [22, 23]. However, the ν(C–N) values did not correspond to the typical ranges of the corresponding single C–N (1250–1360 cm^{-1}) or double C=N (1640–1690 cm^{-1}) bonds. The frequencies of the experimental bands were in between those ranges, closer to the high-frequency part, evidencing partially double character of the formally single N–C(S)S bond [24, 25]. Hence, the obtained data suggested the shorter N–C(S)S bond length in structure **3**.

Moreover, the bands of the thioureid group in the spectra of the gold(III)–mercury(II) complexes were shifted to higher frequency in comparison with the original mercury(II) dithiocarbamates: $[Hg_2\{S_2CN(CH_2)_6\}_4]$ and $[Hg\{S_2CN(CH_2)_4O\}_2]_n$ as well as the corresponding sodium salts. Therefore, we concluded that the rearrangement of the dithiocarbamate groups from the coordination sphere of mercury(II) to that of gold(III) was accompanied by the increase in the contribution of the double bonding and, hence, the shortening of the N–C(S)S bonds in complexes **1** and **3** in comparison with mercury(II) dithiocarbamates.

The absorption bands of medium intensity at 1063 (**1**), 1059 cm^{-1} (**3**) and 972 (**1**), 993 cm^{-1} (**3**) were assigned

to the asymmetric (ν_{as}) and symmetric (ν_s) stretching of the C(S)S groups, respectively [23, 26]. Weak bands at 538–652 cm^{-1} were related to the ν(C–S) vibrations [27]. The 2851–2926 cm^{-1} range contained the absorption bands due to symmetric and asymmetric stretching of the C–H bonds in the methylene groups of the dithiocarbamate ligands. The spectrum of compound **1** contained the band at 749 cm^{-1} assigned to rocking of the CH_2 groups which pointed at the presence of polymethylene chains in the cyclic $–N(CH_2)_6$ fragments, whereas an additional medium-intensity band at 959 cm^{-1} was assigned to the C–C stretching [28]. A strong band with extremum at 1103 cm^{-1} in the spectrum of compound **3** was assigned to the C–O–C polar group stretching in the $N(CH_2)_4O$ six-membered heterocycle [28].

The crystal structures of the obtained compounds were elucidated by means of X-ray diffraction analysis. The unit cells of the heteronuclear ionic-polymeric complexes **1**–**3** contained 4, 2, and 1 formula units, respectively: $[Au\{S_2CN(CH_2)_6\}_2][HgCl_3]$, $[Au\{S_2CN(CH_2)_6\}_2]_2[HgCl_4]\cdot H_2O$, and $[Au\{S_2CN(CH_2)_4O\}_2]_2[Hg_2Cl_6]$ (Table 1, Fig. 2).

In contrast to complex **1**, whose centrosymmetric $[Au\{S_2CN(CH_2)_6\}_2]^+$ cations were structurally equivalent, the gold(III) complex cations in compounds **2** and **3** existed in several isomeric forms, which could be regarded as conformers, performing various structural functions. It should be noted that structure **2** contained both non-centrosymmetric cations **A** (with the Au^1 atom) and the centrosymmetric ones **B** and **C** (Au^2 and Au^3), whereas both isomeric $[Au\{S_2CN(CH_2)_4O\}_2]^+$ cations **A** and **B** (Au^1 and Au^2) in complex **3** were centrosymmetric (Table 2).

The central gold atoms (*dsp*²-hybrid state) formed planar-tetragonal $[AuS_4]$ chromophores in the considered cations, due to the binding of two dithiocarbamate groups of the ligands, coordination of which was close to the S,S'-isobidentate one: the Au–S bond length ranged between 2.3245 and 2.3496 Å (Table 2). Such coordination was accompanied by the formation of two four-membered $[AuS_2C]$ metallocycles combined via a common metal atom. The coplanarity of the atoms in the cyclic fragments was reflected in the AuSSC and SAuCS torsion angles close to 180° (179.8°, 171.8°–178.8°, and 176.0°–177.7° for complexes **1**–**3**, respectively). Certain deviation of the atoms from the plane could be represented at bending of the $[AuS_2C]$ cycles along the S–S axis. The transannular

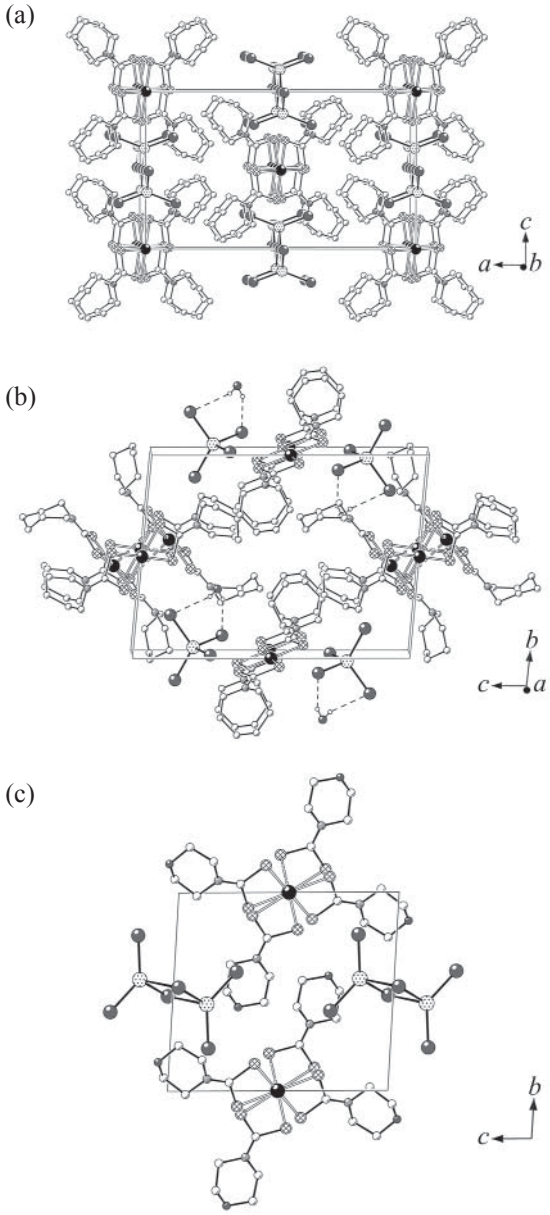

Fig. 2. Packing of structural units in the crystals of compounds **1** (a), **2** (b), and **3** (c).

distances Au–C (2.830, 2.815–2.843, 2.818, and 2.822 Å) and S–S (2.852, 2.850–2.871, 2.858, and 2.868 Å) in complexes **1**–**3** were significantly shorter than the sums of the van der Waals radii of the corresponding pairs of atoms: 3.36 and 3.60 Å [29, 30], evidencing small size of the metallocycles and significantly connivent positions of the gold and carbon atoms.

The SCNC torsion angles of 179.9°–171.5° and 0.1°–7.3° pointed at the close to planar arrangement of the atoms in the $C_2NC(S)S$ moiety of the dithiocarbamate ligands. That fact, along with the higher strength of the

Table 1. Crystallographic data, parameters of experiment and structure refinement for complexes **1**–**3**

Parameter	Value		
	1	**2**	**3**
Empirical formula	$C_{14}H_{24}AuCl_3HgN_2S_4$	$C_{28}H_{50}Au_2Cl_4HgN_4OS_8$	$C_{20}H_{32}Au_2Cl_6Hg_2N_4O_4S_8$
M	852.50	1451.52	1656.79
Crystal system	Monoclinic	Triclinic	Triclinic
Space group	*C*2/*c*	*P*–1	*P*–1
a, Å	20.9361(17)	10.0563(5)	8.0591(4)
b, Å	12.0006(7)	12.7103(7)	10.7044(5)
c, Å	8.8201(5)	17.4503(11)	11.9505(6)
α, deg	90.00	94.268(2)	92.9340(10)
β, deg	97.433(3)	100.991(2)	98.9860(10)
γ, deg	90.00	99.500(2)	93.9650(10)
V, Å^3	2197.4(3)	2146.6(2)	2118.1(2)
Z	4	2	1
d_{calc}, g/cm^3	2.577	2.246	2.714
μ, mm^{-1}	14.395	11.053	15.602
F(000)	1584	1372	760
Crystal size, mm	0.15×0.12×0.03	0.42×0.04×0.01	0.36×0.14×0.02
Data collection range over θ	1.96–27.54	1.92–27.61	1.73–27.60
Indexes range	$-27 \le h \le 26$, $-14 \le k \le 15$, $-9 \le l \le 11$	$-13 \le h \le 12$, $-16 \le k \le 16$, $-22 \le l \le 22$	$-10 \le h \le 10$, $-13 \le k \le 13$, $-1\ 5 \le l \le 15$
Reflections measured	6685	22175	9933
Independent reflections	2545 (R_{int} = 0.0492)	9917 (R_{int} = 0.0386)	4674 (R_{int} = 0.0745)
Reflections with $I > 2\sigma(I)$	1914	7062	4279
Refined parameters	117	442	211
GOOF	1.029	0.977	1.050
R-Factors over $F^2 > 2\sigma(F^2)$	R_1 = 0.0412, wR_2 = 0.0703	R_1 = 0.0401, wR_2 = 0.0816	R_1 = 0.0333, wR_2 = 0.0977
R-Factors over all reflections	R_1 =0.0611, wR_2 = 0.0758	R_1 =0.0706, wR_2 = 0.0887	R_1 =0.0365, wR_2 = 0.0995
Residual electronic density (min/max), *e*/Å^3	–1.654/1.829	–2.108/2.932	–1.837/2.218

N–C(S)S bonds (1.289–1.318 Å) as compared to the N–CH_2 ones (1.459–1.486 Å), resulted from the double character contribution to the formally single bond due to the sp^2 admixing to the sp^3-hybrid state of the nitrogen and carbon atoms. It should be noted that the N–C(S)S bonds in complexes **1** (1.318 Å) and **3** (1.306, 1.307 Å) were noticeably shorter than in the corresponding original mercury(II) complexes: $[Hg_2\{S_2CN(CH_2)_6\}_4]$ 1.326, 1.327 Å [15] and $[Hg\{S_2CN(CH_2)_4O\}_2]_n$ 1.335 Å [18], as was expected from the IR spectroscopy data.

The six-membered $N(CH_2)_4O$ heterocycles (**3**) adopted the *chair* conformation, whereas the seven-membered $N(CH_2)_6$ cycles exhibited either *chair* (**1**) or *twisted chair* (**2**) conformation [31].

Table 2. Selected bond lengths (*d*), bond angles (ω), and torsion angles (φ) in complexes **1**[a], **2**[b], and **3**[c]

Compound **1**			
Cation			
Bond	*d*, Å	Bond	*d*, Å
Au^1–S^1	2.333(2)	N^1–C^7	1.476(10)
Au^1–S^2	2.346(2)	C^2–C^3	1.527(10)
$Au^1\cdots S^{2b}$	3.647(2)	C^3–C^4	1.499(11)
S^1–C^1	1.705(8)	C^4–C^5	1.517(11)
S^2–C^1	1.749(7)	C^5–C^6	1.513(11)
N^1–C^1	1.318(9)	C^6–C^7	1.499(11)
N^1–C^2	1.486(8)		
Angle	ω, deg	Angle	ω, deg
$S^1Au^1S^2$	75.11(7)	$Au^1S^2C^1$	86.1(3)
$S^1Au^1S^{2a}$	104.89(7)	$S^1C^1S^2$	111.3(4)
$Au^1S^1C^1$	87.5(2)		
Angle	φ, deg	Angle	φ, deg
$Au^1S^1S^2C^1$	–179.8(4)	$S^1C^1N^1C^7$	178.2(5)
$S^1Au^1C^1S^2$	–179.8(4)	$S^2C^1N^1C^2$	–175.8(5)
$S^1C^1N^1C^2$	2.2(9)	$S^2C^1N^1C^7$	0.2(9)
Anion			
Bond	*d*, Å	Bond	*d*, Å
Hg^1–Cl^1	2.369(2)	Hg^1–Cl^2	2.7465(3)
Angle	ω, deg	Angle	ω, deg
$Cl^1Hg^1Cl^{1c}$	138.10(11)	$Cl^2Hg^1Cl^{2c}$	106.81(2)
$Cl^1Hg^1Cl^2$	94.18(5)	$Cl^{1c}Hg^1Cl^2$	110.70(6)
Compound **2**			
Cation **A**			
Bond	*d*, Å	Bond	*d*, Å
Au^1–S^1	2.350(2)	N^2–C^9	1.483(8)
Au^1–S^2	2.341(2)	N^2–C^{14}	1.486(8)
Au^1–S^3	2.330(2)	C^2–C^3	1.483(11)
Au^1–S^4	2.327(2)	C^3–C^4	1.516(11)
$Au^1\cdots S^{3a}$	3.493(2)	C^4–C^5	1.517(12)
S^1–C^1	1.739(8)	C^5–C^6	1.522(8)
S^2–C^1	1.747(7)	C^6–C^7	1.512(13)
S^3–C^8	1.728(6)	C^9–C^{10}	1.497(11)
S^4–C^8	1.728(7)	C^{10}–C^{11}	1.536(11)
N^1–C^1	1.289(10)	C^{11}–C^{12}	1.511(11)
N^1–C^2	1.468(9)	C^{12}–C^{13}	1.524(12)
N^1–C^7	1.476(9)	C^{13}–C^{14}	1.526(11)
N^2–C^8	1.302(9)		

Table 2. (Contd.)

Compound **2**			
Cation **A**			
Angle	ω, deg	Angle	ω, deg
$S^1Au^1S^2$	75.48(7)	$Au^1S^1C^1$	86.8(3)
$S^1Au^1S^3$	105.47(6)	$Au^1S^2C^1$	86.8(3)
$S^1Au^1S^4$	178.86(7)	$Au^1S^3C^8$	86.7(2)
$S^2Au^1S^3$	178.92(6)	$Au^1S^4C^8$	86.8(2)
$S^2Au^1S^4$	103.61(6)	$S^1C^1S^2$	110.9(5)
$S^3Au^1S^4$	75.45(6)	$S^3C^8S^4$	111.1(4)
Angle	φ, deg	Angle	φ, deg
$Au^1S^1S^2C^1$	177.6(5)	$S^2C^1N^1C^2$	–177.1(6)
$Au^1S^3S^4C^8$	178.7(4)	$S^2C^1N^1C^7$	–0.5(11)
$S^1Au^1C^1S^2$	177.9(4)	$S^3C^8N^2C^9$	–1.2(9)
$S^3Au^1C^8S^4$	178.8(4)	$S^3C^8N^2C^{14}$	179.9(5)
$S^1C^1N^1C^2$	2.1(11)	$S^4C^8N^2C^9$	179.6(5)
$S^1C^1N^1C^7$	178.8(6)	$S^4C^8N^2C^{14}$	0.7(9)
Cation **B**		Cation **C**	
Bond	*d*, Å	Bond	*d*, Å
Au^2–S^5	2.336(2)	Au^3–S^7	2.341(2)
Au^2–S^6	2.329(2)	Au^3–S^8	2.331(2)
$Au^2\cdots S^{2a}$	3.702(2)	S^7–C^{22}	1.729(8)
S^5–C^{15}	1.735(7)	S^8–C^{22}	1.732(7)
S^6–C^{15}	1.723(8)	N^4–C^{22}	1.311(8)
N^3–C^{15}	1.305(9)	N^4–C^{23}	1.469(9)
N^3–C^{16}	1.473(9)	N^4–C^{28}	1.471(9)
N^3–C^{21}	1.459(9)	C^{23}–C^{24}	1.511(15)
C^{16}–C^{17}	1.534(11)	C^{24}–C^{25}	1.502(15)
C^{17}–C^{18}	1.529(12)	C^{25}–C^{26}	1.491(14)
C^{18}–C^{19}	1.510(8)	C^{26}–C^{27}	1.507(9)
C^{19}–C^{20}	1.488(12)	C^{27}–C^{28}	1.506(12)
C^{20}–C^{21}	1.503(12)		
Angle	ω, deg	Angle	ω, deg
$S^5Au^2S^6$	75.63(7)	$S^7Au^3S^8$	75.23(7)
$S^5Au^2S^{6a}$	104.37(7)	$S^7Au^3S^{8b}$	104.77(7)
$Au^2S^5C^{15}$	86.1(2)	$Au^3S^7C^{22}$	86.5(2)
$Au^2S^6C^{15}$	86.6(2)	$Au^3S^8C^{22}$	86.8(2)
$S^5C^{15}S^6$	111.6(4)	$S^7C^{22}S^8$	111.0(4)
Angle	φ, deg	Angle	φ, deg
$Au^2S^5S^6C^{15}$	178.4(4)	$Au^3S^7S^8C^{22}$	171.8(4)
$S^5Au^2C^{15}S^6$	178.6(4)	$S^7Au^3C^{22}S^8$	172.6(4)
$S^5C^{15}N^3C^{16}$	–7.3(10)	$S^7C^{22}N^4C^{23}$	4.7(10)
$S^5C^{15}N^3C^{21}$	174.9(6)	$S^7C^{22}N^4C^{28}$	–177.3(6)
$S^6C^{15}N^3C^{16}$	171.5(6)	$S^8C^{22}N^4C^{23}$	–178.2(6)
$S^6C^{15}N^3C^{21}$	–6.3(10)	$S^8C^{22}N^4C^{28}$	–0.1(10)
Anion			
Bond	*d*, Å	Bond	*d*, Å
Hg^1–Cl^1	2.468(2)	Hg^1–Cl^3	2.504(2)
Hg^1–Cl^2	2.534(2)	Hg^1–Cl^4	2.467(2)

Table 2. (Contd.)

Compound **2**			
Anion			
Angle	ω, deg	Angle	ω, deg
$Cl^1Hg^1Cl^2$	104.52(7)	$Cl^2Hg^1Cl^3$	110.39(8)
$Cl^1Hg^1Cl^3$	106.40(8)	$Cl^2Hg^1Cl^4$	109.93(7)
$Cl^1Hg^1Cl^4$	116.43(8)	$Cl^3Hg^1Cl^4$	109.02(7)
Compound **3**			
Cation **A**		Cation **B**	
Bond	*d*, Å	Bond	*d*, Å
$Au^1–S^1$	2.3245(14)	$Au^2–S^3$	2.3427(13)
$Au^1–S^2$	2.3435(14)	$Au^2–S^4$	2.3464(14)
$Au^1\cdots S^{4b}$	3.5766(14)	$Au^2\cdots S^1$	3.2998(14)
$S^1–C^1$	1.723(6)	$S^3–C^6$	1.725(6)
$S^2–C^1$	1.734(5)	$S^4–C^6$	1.736(6)
$N^1–C^1$	1.307(7)	$N^2–C^6$	1.306(7)
$N^1–C^2$	1.477(7)	$N^2–C^7$	1.479(7)
$N^1–C^5$	1.463(7)	$N^2–C^{10}$	1.467(7)
$C^2–C^3$	1.523(9)	$C^7–C^8$	1.519(8)
$C^4–C^5$	1.516(9)	$C^9–C^{10}$	1.500(8)
$C^3–O^1$	1.433(7)	$C^8–O^2$	1.429(7)
$C^4–O^1$	1.423(8)	$C^9–O^2$	1.430(7)
Angle	ω, deg	Angle	ω, deg
$S^1Au^1S^2$	75.51(5)	$S^3Au^2S^4$	75.41(5)
$S^1Au^1S^{2a}$	104.49(5)	$S^3Au^2S^{4b}$	104.59(5)
$Au^1S^1C^1$	86.9(2)	$Au^2S^3C^6$	86.5(2)
$Au^1S^2C^1$	86.0(2)	$Au^2S^4C^6$	86.1(2)
$S^1C^1S^2$	111.5(3)	$S^3C^6S^4$	111.9(3)
Angle	φ, deg	Angle	φ, deg
$Au^1S^1S^2C^1$	177.4(3)	$Au^2S^3S^4C^6$	176.0(3)
$S^1Au^1C^1S^2$	177.7(3)	$S^3Au^2C^6S^4$	176.5(3)
$S^1C^1N^1C^2$	–6.9(8)	$S^3C^6N^2C^7$	–4.3(8)
$S^1C^1N^1C^5$	176.9(4)	$S^3C^6N^2C^{10}$	–174.9(4)
$S^2C^1N^1C^2$	172.2(4)	$S^4C^6N^2C^7$	175.0(4)
$S^2C^1N^1C^5$	–3.9(8)	$S^4C^6N^2C^{10}$	4.4(7)
Anion			
Bond	*d*, Å	Bond	*d*, Å
$Hg^1–Cl^1$	2.7106(14)	$Hg^1–Cl^3$	2.3886(15)
$Hg^1–Cl^2$	2.4021(16)	$Hg^1–Cl^{1c}$	2.5693(15)
Angle	ω, deg	Angle	ω, deg
$Cl^1Hg^1Cl^2$	105.54(6)	$Cl^2Hg^1Cl^{1c}$	106.30(6)
$Cl^1Hg^1Cl^3$	96.47(5)	$Cl^3Hg^1Cl^{1c}$	116.89(5)
$Cl^1Hg^1Cl^{1c}$	86.99(4)	$Hg^1Cl^1Hg^{1c}$	93.01(4)
$Cl^2Hg^1Cl^3$	132.22(6)		

Symmetry transformations: [a] (i) $1-x, 1-y, 1-z$; (ii) $1-x, y, 1/2-z$; (iii) $1-x, y, 3/2-z$. [b] (i) $-x, 1-y, -z$; (ii) $-x, -y, 1-z$; (iii) $1-x, 1-y, -z$. [c] (i) $-x, -y, 1-z$; (ii) $1-x, -y, 1-z$; (iii) [c] $-x, 1-y, -z$.

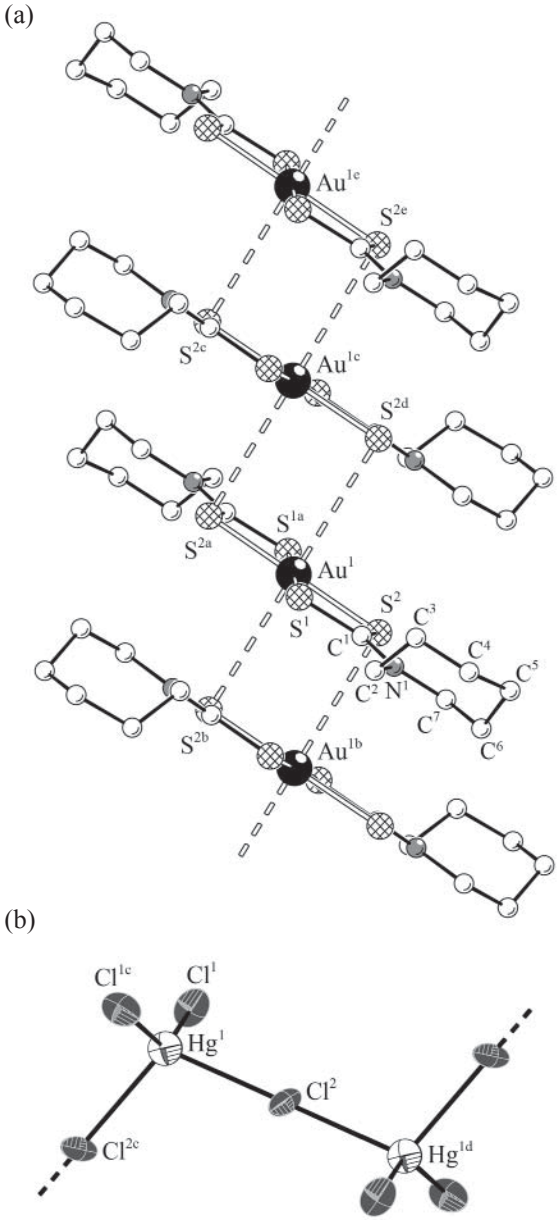

Fig. 3. Fragments of the cationic $([Au\{S_2CN(CH_2)_6\}_2]^+)_n$ (a) and anionic $([HgCl_3]^-)_n$ (b) polymeric chains in compound **1**. (Double dashed lines) show the secondary Au···S bonds between the complex ions.

The anionic part of the considered compounds contained either polymeric complex ion $([HgCl_3]^-)_n$ (**1**) or discrete ions $[HgCl_4]^{2-}$ (**2**) or $[Hg_2Cl_6]^{2-}$ (**3**). The terminal chlorine atoms in the $[HgCl_3]^-$ and $[Hg_2Cl_6]^{2-}$ anions formed much stronger bonds with the central mercury atom than the bridging ones (Table 2). The bridging chlorine atom Cl^2 in each of the $[HgCl_3]^-$ anions symmetrically interacted with the neighbor metal atom, increasing

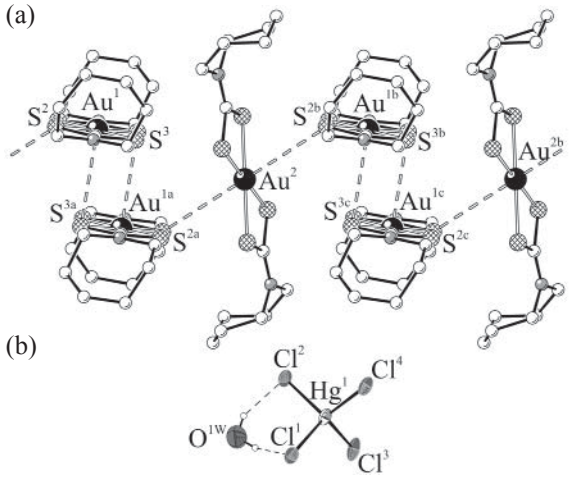

Fig. 4. Fragment of supramolecular cationic chain $(\cdots[\mathbf{A}\cdots\mathbf{A}]\cdots\mathbf{B}\cdots)_n$ in the structure of complex **2** (a) and hydrated anion $[HgCl_4]^{2-}$ (b). The secondary Au···S bonds are shown by double dashed lines; hydrogen bonds are shown by dashed lines.

the coordination number of the latter to 4 and thus forming a zigzag ($Cl^2Hg^1Cl^{2c}$ angle 106.81°) $([HgCl_3]^-)_n$ polymeric chain oriented along the *c* crystal axis (Figs. 2a, 3b).

In the structure of complex **2**, the discrete $[HgCl_4]^{2-}$ anions formed strongly non-equivalent bonds with the outer-sphere H_2O molecules: O–H···Cl^2 3.142 Å and O^1–H···Cl^1 3.414 Å (Fig. 4b). The mercury atoms in structure **3** were combined by the μ_2-Cl^1,Cl^{1c} atoms, thus forming centrosymmetric binuclear $[Hg_2Cl_6]^{2-}$ anions (Fig. 5b): the atoms in the central four-member $[Hg_2Cl_2]$ metallocycle were coplanar, the $Hg^1\cdots Hg^{1c}$ distance being 3.832 Å.

The central mercury atom (sp^3 hybrid state) was in the distorted tetrahedral environment of chlorine atoms each of the considered anions. A convenient parameter to quantitively describe the geometry of the tetrahedral polyhedrons in compounds **1**–**3** was $\tau_4 = [360° - (\alpha + \beta)]/141°$ (α and β being two largest L–M–L angles) [32]. The limiting values of that parameter proposed for the fourfold coordination geometry of the central metal atom pointed to a perfectly tetrahedral ($\tau_4 = 1$; $\alpha = \beta = 109.5°$) or square-tetragonal ($\tau_4 = 0$; $\alpha = \beta = 180°$) structures. The data in Table 2 showed that the τ_4 values were 0.789, 0.945, and 0.787 for complexes **1**–**3**, respectively. Hence, the most regular tetrahedron was realized in the case of tetrachloromercurate(II) ion (**2**); for other two compounds, the contribution of the tetrahedral structure to the polyhedron geometry was close to 79%.

A single type of the nonvalent secondary bonds[2] (Au···S) was realized in compounds **1**–**3**. Nevertheless, their supramolecular organization was significantly different. For example, pairs of symmetrical $Au^{1}\cdots S^{2b}$ and $Au^{1b}\cdots S^{2}$ 3.647 Å secondary bonds in structure **1** combined the equivalent gold(III) cations in linear polymeric chains $([Au\{S_2CN(CH_2)_6\}_2]^+)_n$, the Au···Au distance being 4.410 Å (Figs. 2a, 3a). The cations adjacent along the chain were arranged so that the bisecting planes passing through the $[CS_2AuS_2C]$ bicyclic fragments formed an angle close to the right one, 86.37° (Fig. 2a). The alternating cationic and anionic polymeric chains in the crystal structure **1** were oriented along the *c* crystal axis (Fig. 2a).

The non-centrosymmetric isomeric cations **A** in complex **2** were involved in the pairwise $Au^{1}\cdots S^{3a}$ and $Au^{1a}\cdots S^{3}$ 3.493 Å secondary interactions, thus forming the $[Au_2\{S_2CN(CH_2)_6\}_4]^{2+}$ supramolecular dications containing the $[Au\{S_2CN(CH_2)_6\}_2]^+$ mononuclear fragments in the antiparallel orientation, the Au^{1}–Au^{1a} intradimer distance being 4.019 Å (Fig. 4a). The weaker secondary bonds ($S^{2a}\cdots Au^{2}$ 3.702 Å) between each of the discussed binuclear cations with the neighbor centrosymmetric cations **B** led to the formation of the zigzag supramolecular chains $(\cdots[\mathbf{A}\cdots\mathbf{A}]\cdots\mathbf{B}\cdots)_n$ containing the binuclear and mononuclear cations alternating along the chain: the $Au^{1}Au^{1}Au^{2}$ and $Au^{1}Au^{2}Au^{1}$ angles were 85.55° and 180°, respectively, and the $Au^{1}\cdots Au^{2}$ interatomic distance was 4.768 Å (Fig. 4a). The centrosymmetric discrete cations **C** were located between the chains (Fig. 2b). Let us note evident effect of the Au···S secondary bonds on the spatial orientation of the bulky $N(CH_2)_6$ cyclic fragments. For example, the pairs of the cyclic fragments in the $[Au_2\{S_2CN(CH_2)_6\}_4]^{2+}$ supramolecular binuclear cations showed opposite orientation, due to the interligand repulsion forces (Fig. 4a); the cyclic fragments in each cation were located to the same side with respect to the $[AuS_4]$ chromophore plane (*cis*-orientation). On the contrast, the considered heterocycles revealed *trans*-orientation in the mononuclear cations **B** and **C**.

Two isomeric centrosymmetric cations $[Au\{S_2CN(CH_2)_4O\}_2]^+$ were alternated in the supramolecular cationic chains of complex **3**: **A** and **B** (the $Au^{1}\cdots Au^{2}$ interatomic distance 4.030 Å). For each of the cations, the observed secondary interactions involved the gold atom and two diagonal sulfur atoms. The length of

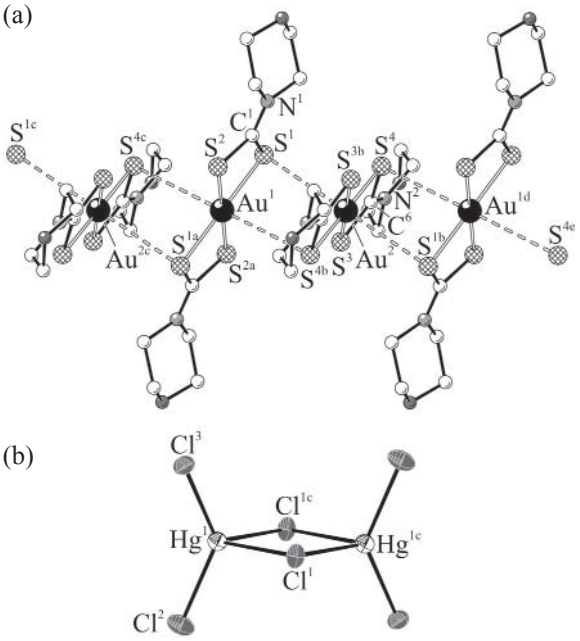

Fig. 5. Fragment of polymeric cationic chain $(\cdots\mathbf{A}\cdots\mathbf{B}\cdots)_n$ (a) and structure of binuclear anion $[Hg_2Cl_6]^{2-}$ (b) in compound **3**. The secondary Au···S bonds between the isomeric cations are shown by double dotted lines.

the Au···S secondary bonds formed by the nonequivalent gold atoms was different: $Au^{1}\cdots S^{4}$ 3.5766 Å and $Au^{2}\cdots S^{1}$ 3.2998 Å (for comparison, the sum of van der Waals radii of gold and sulfur atoms equals 3.46 Å [29, 30]). Hence, the formation of the linear supramolecular chain $(\cdots\mathbf{A}\cdots\mathbf{B}\cdots)_n$ oriented along the *a* crystal axis presumed the formation of two pairs of asymmetrical secondary bonds between each cation and the closest neighbors (Fig. 5a). The mutual spatial orientation of the neighbor cations could be characterized by the angle of 74.19° between their bisecting planes passing through the $[CS_2AuS_2C]$ bicyclic fragments.

The Au···S additional secondary interactions in supramolecular structures **1**–**3** led to the transformation of the $[AuS_4]$ coordination polyhedron to the elongated tetragonal pyramid $[AuS_5]$ (**2**, Au^{1}) or elongated octahedron $[AuS_6]$. The vertex sulfur atoms in those polyhedrons were shifted from the ideal positions, since the S···Au–S angles deviated from 90°. The $S^{3a}Au^{1}S^{2}$ angle in the distorted pyramid equaled 85.34° (Fig. 4a); the corresponding angles for the octahedrons in complexes **1**–**3** were as follows: $S^{2b}Au^{1}S^{1}$ 84.74°, $S^{2b}Au^{2}S^{5}$ 68.56°, $S^{4c}Au^{1}S^{2}$ 86.78°, and $S^{1}Au^{2}S^{4}$ 86.37° (Figs. 3a–5a).

Thermal behavior of the complexes was studied by means of simultaneous thermal analysis involving

[2] The concept of secondary bonds was introduced for the first time in [33] to describe the interactions at the distance comparable to the sum of van der Waals radii of the corresponding pairs of atoms.

synchronous recording of thermogravimetry (TG) and differential scanning calorimetry (DSC) curves. Thermal behavior of the studied substances was similar, as revealed by the TG curves reflecting the formally single-stage thermolysis. The major mass loss of complexes **1** and **3** (64.00 and 66.69%) corresponded to the temperature ranges of ~195–340 and ~230–365°C, respectively. Differentiation of those steeply descending sections of the TG curves revealed the inflection points at 230.0 and 258.0°C, respectively, pointing at the complex thermolysis of the cations and anions simultaneously. Thermolysis of the cationic part of the complexes led to the reduction of gold(III) into elemental gold; heat-induced decomposition of the anionic part was accompanied by the release of $HgCl_2$ (followed by its evaporation). The high-temperature parts of the TG curves at ~340–935 and ~365–850°C reflected steady desorption of 12.49 and 6.98% of the volatile products, respectively. The residual mass at 1100°C [22.89 (**1**) and 25.96% (**3**)] was close to the one expected for reduced gold [calculated 23.10 (**1**) and 23.78% (**3**)] which was almost quantitatively regenerated under relatively mild conditions. Small spherical particles of metal gold were observed during the crucibles examination.

The low-temperature part of the DSC curve for complex **1** contained two weak endothermal effects, one of them (extremum at 168.0°C) reflected the specimen meting (extrapolated mp = 162.5°C; melting without signs of decomposition was independently determined at 168–170°C using a glass capillary), whereas the second one (extremum at 260.9°C) was assigned to vigorous thermolysis of the sample and evaporation of the decomposition products. The low-temperature part of the DSC curve for compound **3** showed a single strong endothermal effect at 256.7°C (extrapolated process temperature 254.6°C) corresponding to the major mass loss stage and assigned to thermal decomposition of the complex. Even though the DSC curve did not show the endothermal melting effect distinctly, the phase transition was observed in a glass capillary at 252–254°C. The high-temperature part of the DSC curves contained an endothermal effect of elemental gold melting: extrapolated mp = 1062.3 and 1062.6°C.

In summary, we prepared, isolated, and characterized by means of X-ray diffraction analysis the novel crystalline ionic-polymeric Au(III)–Hg(II) complexes $([Au\{S_2CN(CH_2)_6\}_2]\cdot[HgCl_3])_n$, $([Au\{S_2CN(CH_2)_6\}_2]_2[HgCl_4]\cdot H_2O)_n$, and $([Au\{S_2CN(CH_2)_4O\}_2]_2[Hg_2Cl_6])_n$ containing three types of polychloro(di)mercurate(II) ions. The Au···S secondary interactions determined the supramolecular self-assembly of the obtained substances. The study of thermal behavior of the complexes revealed the conditions of quantitative regeneration of the bound gold, $HgCl_2$ being the byproduct of thermolysis.

EXPERIMENTAL

IR spectra were recorded using a PerkinElmer Spectrum 65 Fourier spectrometer (ATR, 400–4000 cm^{-1}). Dispersion state and morphology of the samples were studied by means of high-resolution scanning electron microscopy using a JSM 6390LV JEOL microscope (Japan) equipped with an Oxford INCA Energy 350-Wave (England) microanalysis system with dispersion over energy and wavelength. Qualitative chemical composition was determined using a microprobe technique with an energy-dispersive spectrometer). Thermal behavior of complexes **1** and **3** was studied by means of simultaneous thermal analysis (TG and DSC) using a STA 449C Jupiter NETZSCH instrument (corundum crucible, heating rate 5 deg/min up to 1100°C, argon atmosphere, specimen mass 1.828–5.424 mg; accuracy of temperature and mass reading ±0.4°C and $\pm 1\times10^{-4}$ mg). The correction file recorded with an empty crucible was used during the data processing; the instrument was calibrated with respect to temperature and sensitivity prior to the measurement. Melting points were determined independently using a PTP(M) instrument (Khimlabpribor, Russia). Elemental analysis was performed using a Euro EA-3000 automated analyzer. Gold content was determined using an iCE 3000 atomic absorption spectrometer (Thermo Electron Corporation, USA). Degree of gold binding from the solutions (S, %) was calculated as $S = [(c - c_r)/c]\times100\%$, c and c_r being starting and residual content of gold in the solution, respectively.

X-ray diffraction analysis of monocrystals **1**–**3** was performed using a Bruker-Nonius X8 Apex CCD diffractometer (MoK_α radiation, λ = 0.71073 Å, graphite monochromator) at 296(2) (**1**) and 150(2) K (**2**, **3**). Data collection was performed using a conventional procedure of φ and ω narrow frames scanning. Absorption was accounted for using SADABS software [34]. The structures were solved via direct method and refined via least squares method (over F^2) under full-matrix anisotropic approximation for non-hydrogen atoms. Positions of hydrogen atoms were calculated from geometry and included in the refinement using a *riding* model. Hydrogen atoms of the hydrated water molecules in compound **2** were localized via differential synthesis of the electron

density and refined under isotropic approximation with $U_{iso}(H) = 1.5U_{eq}(O)$ and distances O–H = 0.89(2) Å and H···H = 1.45(2) Å. Data collection and processing as well as refinement of unit cell parameters were performed using APEX2 [34] and SAINT software [34]. Structure refinement was performed using SHELXTL software package [34]. Atomic coordinates, bond lengths, and bond angles were deposited at the Cambridge Crystallographic Data Centre [CCDC 1905389 (**1**), 1905390 (**2**), and 1905391 (**3**)].

The initial sodium salts, $Na(S_2CNR_2)\cdot 2H_2O$, were prepared via the interaction of carbon sulfide (Merck) with the corresponding cyclic N-donor base, hexamethyleneimine or morpholine (Aldrich) in an alkaline medium [22].

$Na\{S_2CN(CH_2)_6\}\cdot 2H_2O$. IR spectrum, ν, cm^{-1}: 3369, 3295, 3167, 2983, 2923, 2851, 2105, 1638, 1622, 1484, 1448, 1429, 1407, 1366, 1339, 1283, 1258, 1244, 1187, 1168, 1095, 1067, 1046, 1009, 972, 953, 904, 850, 828, 764, 736, 678, 624, 562, 530, 479, 454, 440, 408.

$Na\{S_2CN(CH_2)_4O\}\cdot 2H_2O$. IR spectrum, ν, cm^{-1}: 3350, 3271, 3190, 2966, 2903, 2853, 2469, 2112, 1641, 1623, 1585, 1458, 1417, 1385, 1347, 1323, 1300, 1260, 1211, 1182, 1110, 1063, 1023, 976, 894, 871, 825, 676, 634, 577, 540, 482, 443, 420, 411, 403.

The mercury(II) dithiocarbamate complexes, $[Hg_2\{S_2CN(CH_2)_6\}_4]$ [15] and $[Hg\{S_2CN(CH_2)_4O\}_2]_n$ [18], were prepared via quantitative precipitation of Hg^{2+} ions from an aqueous phase with the corresponding sodium dithiocarbamates taken in 5% excess.[3]

$[Hg_2\{S_2CN(CH_2)_6\}_4]$. IR spectrum, ν, cm^{-1}: 2977, 2921, 2850, 1496, 1479, 1455, 1421, 1342, 1285, 1261, 1243, 1193, 1157, 1090, 1050, 1003, 990, 975, 952, 906, 875, 847, 826, 806, 765, 746, 619, 573, 536, 514, 489, 471, 439, 420, 402.

$[Hg\{S_2CN(CH_2)_4O\}_2]_n$. IR spectrum, ν, cm^{-1}: 2968, 2910, 2871, 1468, 1455, 1441, 1423, 1346, 1318, 1300, 1259, 1223, 1205, 1116, 1070, 1023, 993, 900, 873, 821, 653, 555, 536, 439, 420, 411, 402.

Complexes 1–3 (*general procedure*). 10 mL of $AuCl_3$ solution in 2 M. HCl containing 35.3 (**1**, **2**) or 37.2 mg (**3**) of gold was added to freshly precipitated mercury(II) dithiocarbamates (100 mg), and the mixture was stirred during 30 min. Analysis of the solutions upon the interaction revealed the binding degree of gold from the solution of 99.9 (**1**, **2**) and 99.7% (**3**). The formed yellow precipitates were filtered off, washed, and dried on a filter. Yield 98.4 (**1**, **2**) and 98.9% (**3**). To prepare suitable single crystals for X-ray diffraction analysis, the substance isolated from the $[Hg_2\{S_2CN(CH_2)_6\}_4]$–$H[AuCl_4]$/2 M HCl chemisorption system was dissolved in acetone. The small amount of needle-like crystals of compound **2** were picked out from the mass of yellow platelet crystals of complex **1** obtained via slow evaporation of the solvent. Yellow platelet crystals of complex **3** were grown from methanol.

Bis(N,N-cyclohexamethylenedithiocarbamato-S,S')gold(III) trichloromercurate(II) (1). IR spectrum, ν, cm^{-1}: 2977, 2919, 2851, 1522, 1499, 1463, 1428, 1351, 1270, 1232, 1200, 1177, 1158, 1096, 1064, 972, 959, 913, 866, 846, 819, 749, 611, 564, 511, 458, 438, 427, 420, 406. Found, %: C 20.7; H 2.8; N 3.4; S 15.1. $C_{14}H_{24}AuCl_3HgN_2S_4$. Calculated, %: C 19.72; H 2.84; N 3.29; S 15.04.

Bis(morpholinedithiocarbamato-S,S')gold(III) hexachlorodimercurate(II) (3). IR spectrum, ν, cm^{-1}: 2987, 2926, 2858, 1537, 1459, 1423, 1383, 1356, 1297, 1267, 1243, 1212, 1103, 1059, 1019, 993, 878, 826, 652, 538, 456, 440, 428, 420, 411, 405. Found, %: C 14.7; H 1.9; N 3.4; S 15.7. $C_{20}H_{32}Au_2Cl_6Hg_2N_4O_4S_8$. Calculated, %: C 14.50, H 1.95, N 3.38, S 15.48.

ACKNOWLEDGMENTS

Electron microscopy studies, determination of gold content in the solutions, and recording of energy-dispersive spectra were performed at the Analytical Center for Mineralogy and Geochemical Studies, Institute of Geology and Nature Management, Far Eastern Branch of the RAS. IR spectra were recorded at the Center For Collective Usage, Kurnakov Institute of General and Inorganic Chemistry, Russian Academy of Sciences.

CONFLICT OF INTEREST

No conflict of interest was declared by the authors.

REFERENCES

1. Kloppers, L., Maree, W., Oyekola, O., and Hangone, G., *Miner. Engin*., 2016, vol. 87, p. 54. https://doi.org/10.1016/j.mineng.2015.12.003
2. Nieuwenhuizen, P.J., *Appl. Catal. (A)*, 2001, vol. 207, nos. 1–2, p. 55. https://doi.org/10.1016/S0926-860X(00)00613-X
3. Onwudiwe, D.C. and Ajibade, P.A., *Mater. Lett*., 2011, vol. 65, no. 21–22, p. 3258. https://doi.org/10.1016/j.matlet.2011.07.012
4. Sathiyaraj, E. and Thirumaran, S., *Spectrochim. Acta (A)*, 2012, vol. 97, p. 575. https://doi.org/10.1016/j.saa.2012.06.052

[3] It is important to note that heteroleptic polymeric and polynuclear complexes: $[Hg_2\{S_2CN(iso\text{-}C_3H_7)_2\}_2Cl_2)]_n$ [35], $[Hg_4\{S_2CN(C_3H_7)_2\}_6(NO_3)_2]_n$ [36] and cyclic $[Hg_4\{S_2CN(C_3H_7)_2\}_4Cl_4]$ [36] could be formed in the HgX_2–$R_2NC(S)S^-$–H_2O (X = Cl, NO_3) systems, besides the mercury(II) dithiocarbamates themselves.

5. Srinivasan, N. and Thirumaran, S., *Superlatt. Microstruct*., 2012, vol. 51, no. 6, p. 912. https://doi.org/10.1016/j.spmi.2012.03.006
6. Nami, S.A.A., Husain, A., and Ullah, I., *Spectrochim. Acta (A)*, 2014, vol. 118, p. 380. https://doi.org/10.1016/j.saa.2013.08.064
7. Prakasam, B.A., Lahtinen, M., Peuronen, A., Muruganandham, M., Kolehmainen, E., Haapaniemi, E., and Sillanpää, M., *Mater. Lett*., 2015, vol. 144, p. 19. https://doi.org/10.1016/j.matlet.2014.12.128
8. Hrubaru, M., Onwudiwe, D.C., and Hosten, E., *J. Sulfur Chem*., 2016, vol. 37, no. 1, p. 37. https://doi.org/10.1080/17415993.2015.1080707
9. Chesman, A.S.R., van Embden, J., Duffy, N.W., Webster, N.A.S., and Jasieniak, J.J., *Cryst. Growth Des*., 2013, vol. 13, p. 1712. https://doi.org/10.1021/cg4000268
10. Ronconi, L., Giovagnini, L., Marzano, C., Bettìo, F., Graziani, R., Pilloni, G., and Fregona, D., *Inorg. Chem*., 2005, vol. 44, no. 6, p. 1867. https://doi.org/10.1021/ic048260v
11. Ronconi, L., Marzano, C., Zanello, P., Corsini, M., Miolo, G., Maccà, C., Trevisan, A., and Fregona, D., *J. Med. Chem*., 2006. Vol.49, no. 5, p. 1648. https://doi.org/10.1021/jm0509288
12. Milacic, V., Chen, D., Ronconi, L., Landis-Piwowar, K.R., Fregona, D., and Dou, Q.P., *Cancer Res*., 2006, vol. 66, no. 21, p. 10478. https://doi.org/10.1158/0008-5472.CAN-06-3017
13. Mansour, M.A., Connick, W.B., Lachicotte, R.J., Gysling, H.J., and Eisenberg, R., *J. Am. Chem. Soc*., 1998, vol. 120, no. 6, p. 1329. https://doi.org/10.1021/ja973216i
14. Han, S., Jung, O.-S., and Lee, Y.-A., *Trans. Met. Chem*., 2011, vol. 36, no. 7, p. 691. https://doi.org/10.1007/s11243-011-9521-z
15. Ivanov, A.V., Korneeva, E.V., Bukvetskii, B.V., Goryan, A.S., Antzutkin, O.N., and Forsling, W., *Russ. J. Coord. Chem*., 2008, vol. 34, no. 1, p. 59. https://doi.org/10.1007/s11173-008-1010-3
16. Loseva, O.V., Rodina, T.A., Antzutkin, O.N., and Ivanov, A.V., *Russ. J. Gen. Chem*., 2018, vol. 88, no. 12, p. 2540. https://doi.org/10.1134/S1070363218120149
17. Loseva, O.V., Rodina, T.A., Smolentsev, A.I., and Ivanov, A.V., *Polyhedron*, 2017, vol. 134, p. 238. https://doi.org/10.1016/j.poly.2017.06.021
18. Loseva, O.V., Rodina, T.A., and Ivanov, A.V., *Russ. J. Coord. Chem*., 2019, vol. 45, no. 1, p. 22. https://doi.org/10.1134/S1070328419010068
19. Jotani, M.M., Tan, Y.S., and Tiekink, E.R.T., *Z. Kristallogr*., 2016, vol. 231, no. 7, p. 403. https://doi.org/10.1515/zkri-2016-1943
20. Howie, R.A., Tiekink, E.R.T., Wardell, J.L., and Wardell, S.M.S.V., *J. Chem. Crystallogr*., 2009, vol. 39, no. 4, p. 293. https://doi.org/10.1007/s10870-008-9473-0
21. Loseva, O.V., Rodina, T.A., Smolentsev, A.I., and Ivanov, A.V., *Russ. J. Coord. Chem*., 2016, vol. 42, no. 11, p. 719. https://doi.org/10.1134/S1070328416110063
22. Byr'ko, V.M., *Ditiokarbamaty* (Dithiocarbamates), Moscow: Nauka, 1984.
23. Bellamy, L.J., *The Infrared Spectra of Complex Molecules*, New York: Wiley, 1958.
24. Casas, J.S., Sanchez, A., Bravo, J., Soledad, G.F., Castellano, E.E., and Jones, M.M., *Inorg. Chim. Acta*, 1989, vol. 158, no. 1, p. 119. https://doi.org/10.1016/S0020-1693(00)84021-9
25. Ehsan, M.A., Khaledi, H., Tahir, A.A., Ming, H.N., Wijayantha, K.G.U., and Mazhar, M., *Thin Solid Films*, 2013, vol. 536, p. 124. https://doi.org/10.1016/j.tsf.2013.03.092
26. Yin, H., Li, F., and Wang, D., *J. Coord. Chem*., 2007, vol. 60, no. 11, p. 1133. https://doi.org/10.1080/00958970601008846
27. Khitrich, N.V. and Seifullina, I.I., *Russ. J. Coord. Chem*., 2000, vol. 26, no. 11, p. 798.
28. Kazitsyna, L.A. and Kupletskaya, N.B., *Primenenie UF-, IK-, YaMR- i mass-spektroskopii v organicheskoi khimii* (The Use of UV, IR, NMR, and Mass Spectroscopy in Organic Chemistry), Moscow: Mosk. Univ., 1979.
29. Pauling, L., *The Nature of the Chemical Bond and the Structure of Molecules and Crystals*, London: Cornell Univ. Press, 1960.
30. Bondi, A., *J. Phys. Chem*., 1964, vol. 68, no. 3, p. 441. https://doi.org/10.1021/j100785a001
31. Bocian, D.F., Pickett, H.M., Rounds, T.C., and Strauss, H.L., *J. Am. Chem. Soc*., 1975, vol. 97, no. 4, p. 687. https://doi.org/10.1021/ja00837a001
32. Yang, L., Powel, D.R., and Houser, R.P., *Dalton Trans*., 2007, no. 9, p. 955. https://doi.org/10.1039/b617136b
33. Alcock, N.W., *Adv. Inorg. Chem. Radiochem*., 1972, vol. 15, no. 1, p. 1. https://doi.org/10.1016/S0065-2792(08)60016-3
34. Bruker, APEX2 (version 1.08), SAINT (version 7.03), SADABS (version 2.11), SHELXTL (version 6.12). Madison (WI, USA): Bruker AXS Inc., 2004.
35. Angeloski, A., Rawal, A., Bhadbhade, M., Hook, J.M., Schurko, R.W., and McDonagh, A.M., *Cryst. Growth Des*., 2019, vol. 19, no. 2, p. 1125. https://doi.org/10.1021/acs.cgd.8b01619
36. Loseva, O.V., Rodina, T.A., Ivanov, A.V., Smolentsev, A.I., and Antzutkin, O.N., *Russ. Chem. Bull*., 2019, vol. 68, no. 4, p. 782. https://doi.org/10.1007/s11172-019-2486-3